Supporting Information

A versatile foaming platform to fabricate high dielectric permittivity, ultra-low dielectric loss of polymer/carbon composites

Biao Zhao, † Mahdi Hamidinejad, † Chongxiang Zhao, Ruosong Li, Sai Wang, Yasamin Kazemi, Chul B. Park *

Microcellular Plastics Manufacturing Laboratory, Department of Mechanical and Industrial Engineering, University of Toronto, 5 King's College Road, Toronto M5S 3G8, Canada

* Corresponding Author: Chul B. Park, park@mie.utoronto.ca, Tel: +1- 416-978-3053, Fax: +1- 416-978-7753.

2.1 Materials

The PVDF (molecular weight 300,000–330,000 g/mol) was supplied by Solvay. The MWCNTs (NC7000^{TM}) were purchased from Nanocyl SA. The GnPs were supplied by Group Nanoxplore, Inc. (*N,N)*-Dimethylformamide (DMF) was provided by Caledon Laboratories Ltd. The raw materials were used as is, without further purification.

2.2 Fabrication of PVDF/Carbon Solid Composites

The PVDF/carbon (CNTs or GnPs) solid composites were prepared by solvent casting. This was followed by compression-molding, which is similar to the method

previously reported to fabricate PVDF/Ni and PVDF/carbon/Ni composite films. [1-3] In our study, designated amounts of carbon materials (0.2 wt% CNTs or 2.0 wt% GnPs) were uniformly dispersed in the DMF solution using the ultrasonication process. These contents were chosen near the percolation threshold (0.31 wt% CNTs and 5.0 wt% GnPs obtained for the same materials in our previous study) [1] without exceeding it, as mentioned above. Then, the PVDF particles were dissolved by magnetic stirring in the DMF mixture. Finally, the PVDF/carbon (CNTs or GnPs) solid composites were obtained through the evaporation and compression-molding processes.

2.3 Fabrication of PVDF/Carbon Composite Foams

We used a homemade batch foaming device, which is shown in Figure S1, to prepare the PVDF/carbon samples' foaming behavior. The foaming system consisted of a syringe pump filled with CO_2 as the physical blowing agent, and a foaming chamber with a thermal couple to detect the temperature, along with a heater and a depressurizing valve. At the experiment's beginning, we heated the chamber to the desired temperature, and the sample (25 mm× 15 mm× 12 mm) was laid inside it. Subsequently, the CO_2 was quickly released in and out of the chamber so as to eliminate the air. Then, the CO_2 was pressurized into 2,000 psi (13.8 MPa) at an experimental temperature and was held there for one hour. The pressure was quickly released, and the chamber was quenched in cold water. Finally, the sample was

removed from the chamber. We investigated the various foaming temperatures in the ranges of 165.5°C to 167.5°C for the PVDF/CNT and from 167°C to 169°C for the PVDF/GnP composites. The foams prepared at various saturation temperatures (ranging from 165.5°C to 167.5°C for the PVDF/CNT composites, and from 167°C to 169°C for the PVDF/GnP composites) were conveniently denoted as FN1-FN5 and FG1-FG5, respectively, as shown in Table S1.

2.4 Characterization

The densities of the solid (ρ_s) and foam (ρ_f) composites were measured using the water displacement method (the ASTM D792-00). The cell density was calculated based on scanning electron microscopy (SEM) images using the following formula: [4, 5]

$$\text{Cell density} = (n/A)^{3/2} \cdot (\rho_s/\rho_f) \quad (1)$$

where n is the number of cells in the designated area (A) in the SEM micrograph, respectively. The volume expansion ratio was determined as ρ_s/ρ_f.

The crystal structure and phase purity of all the samples was confirmed by x-ray diffraction (XRD, Rigaku Ultima IV, Cu Kα radiation, λ = 0.15418 nm), which was operated at 40 kV and 15 mA. The morphologies of the PVDF-based foam samples were examined using the SEM (JSM-6060) and a field emission scanning electron microscope (FESEM, JSM7001). Fourier transform infrared (FT-IR) spectra of all

samples were recorded in the 700–1,500 cm^{-1} range with a Nicolet 6700 spectrometer. Transmission electron microscopy imaging was carried out with a transmission electron microscope (TEM, JEOL JEM 2010).

Similar to our group's previous measurements, [6-10] an Alpha-A high-performance conductivity analyzer by Novocontrol Technologies GmbH & Co. KG was used to measure the electrical conductivity, the dielectric permittivity, and the dielectric loss of the foamed composites at a voltage of 1 V and a frequency range of $1.0 – 3.0\times10^{5}$ Hz. Prior to dielectric measurements, gold electrodes were deposited onto both surfaces of the specimens by sputtering. To avoid the measurement error, at least four replications were carried out at each sample, and the average values were analyzed in this manuscript.

Table S1 Expansion ratio of PVDF/0.2wt% CNT and PVDF/2wt% GnP foams obtained at various saturation temperatures

Sample	PVDF/0.2wt% CNT composite					PVDF/2wt% GnP composite				
Foam	FN1	FN2	FN3	FN4	FN5	FG1	FG2	FG3	FG4	FG5
Temperature (°C)	165.5	166	166.5	167	167.5	167	167.5	168	168.5	169
Expansion ratio	2.6	4.0	7.2	10	5.8	2.1	2.5	4.4	4.0	2.7

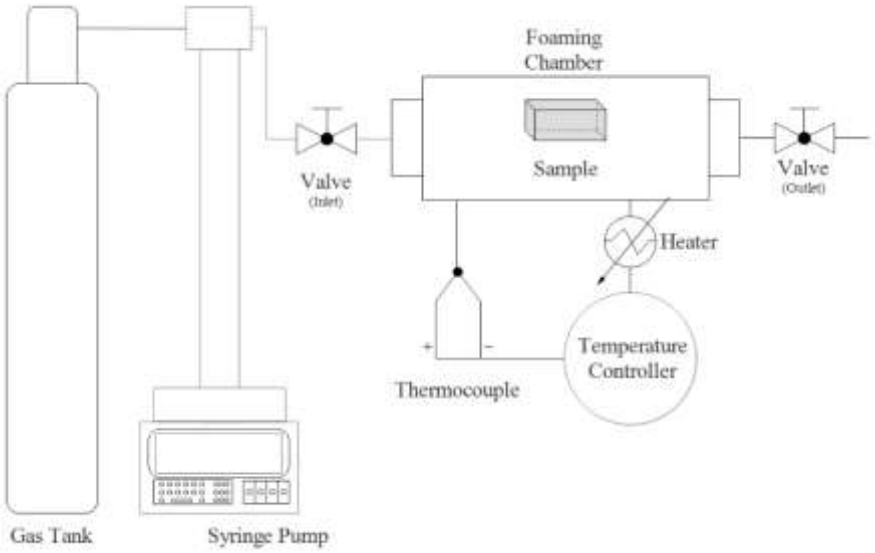

Figure S1 A schematic illustration of the home-made batch-foaming device.

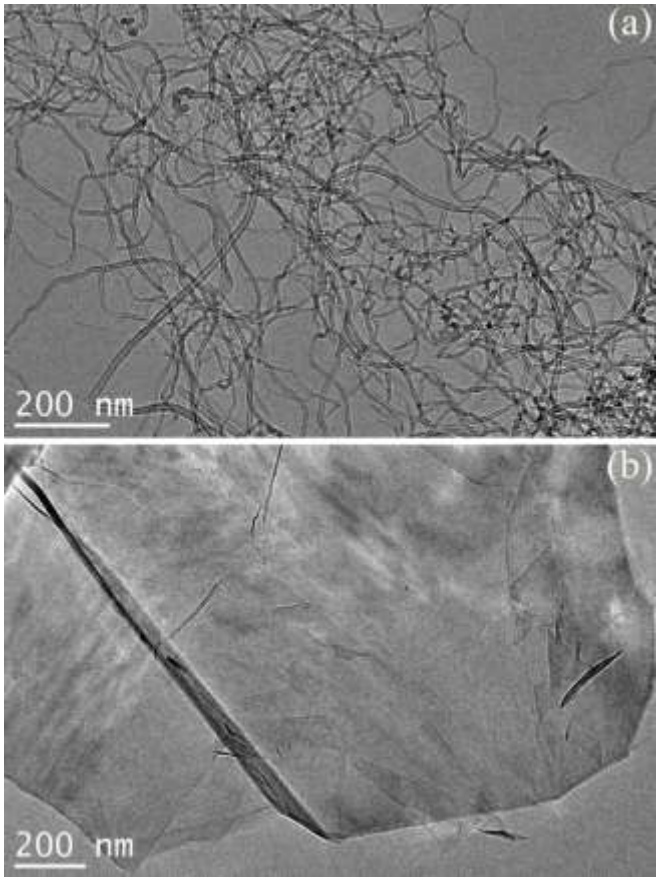

Figure S2 TEM images of (a) CNTs and (b) GnPs.

Figure S2a shows TEM images of the as received CNTs and GnPs. Raw MWCNTs were about 10–30 nm in diameter and 10–15 μm in length. Figure S2b shows the crumbled and encapsulated morphologies of the GnP sample. To examine how the CNTs and GnPs were distributed in the PVDF matrix, we used SEM and TEM techniques to observe the PVDF/carbon materials' morphologies. Figure S3 shows the results. Based on the SEM and TEM images, we expected that the CNTs (Figure S3 (a and b)) and GnPs (Figure S3 (c and d)) had been uniformly distributed in the PVDF matrix.

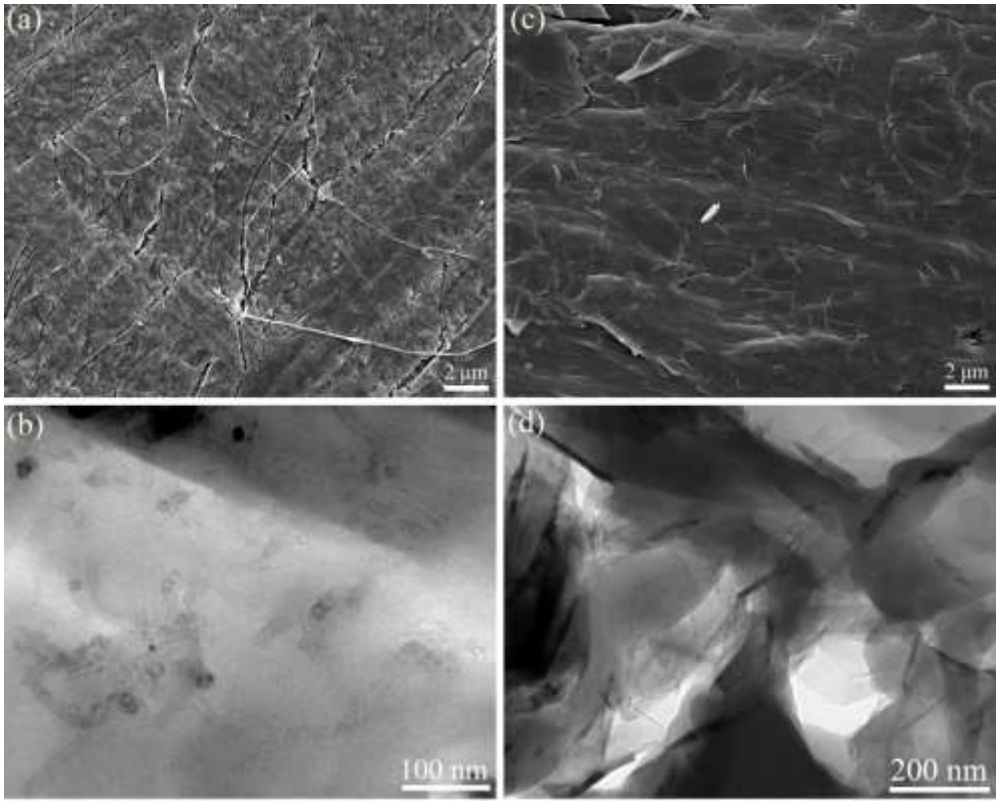

Figure S3 (a and b) SEM and TEM images of PVDF/CNT composites, (c and d) SEM and TEM images of PVDF/GnP composites

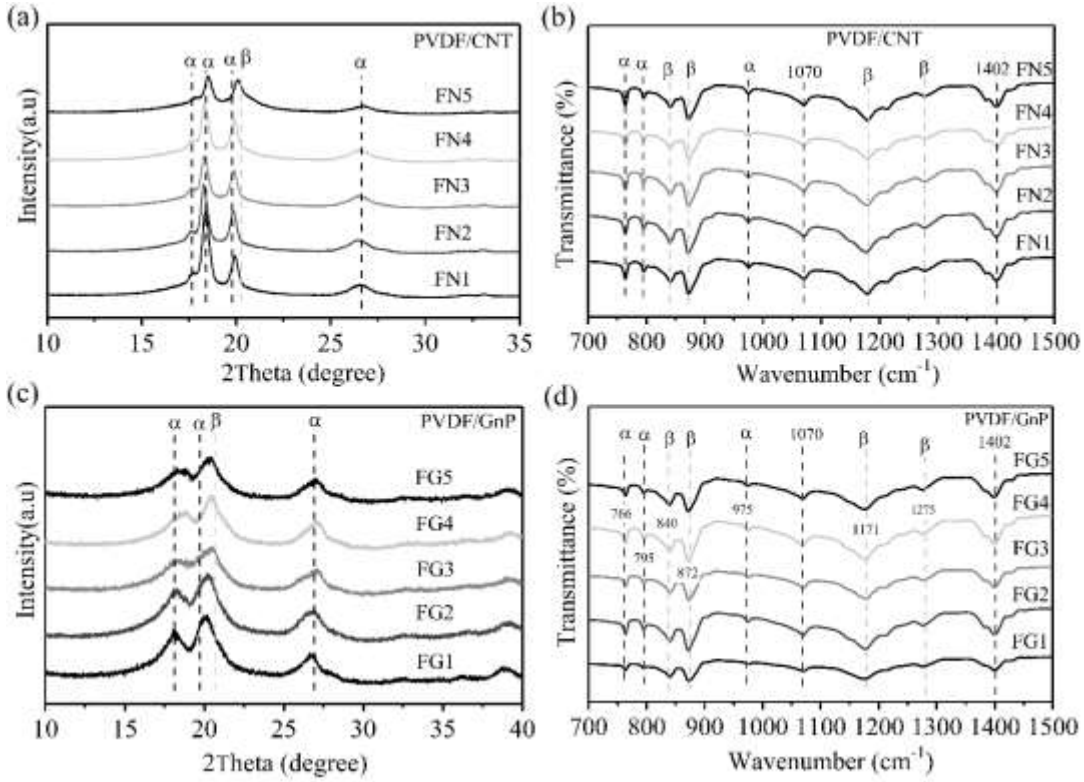

Figure S4 (a) XRD patterns and (b) FT-IR spectra of different PVDF/CNTs composite foams; (c) XRD patterns and (d) FT-IR spectra of PVDF/GnP composite foams.

We carried out X-ray diffraction experiments on the PVDF/CNT and PVDF/GnP composite foams to observe the crystal phase in the PVDF/carbon composite foams, as Figure S4 (a and c) shows. The PVDF/carbon composite foams had several major crystalline peaks that corresponded with the α phase. The peak appeared at 2θ =20.2±0.2º and corresponded with the (1 1 0) and (2 0 0) reflections of the β phase. [11] Thus, the α and β phases coexisted in the PVDF/carbon composite foams. Compared with the neat PVDF, which had only an α phase, the peaks of the α phase in PVDF/carbon composite foams grew rather weak, which meant that the α phase content had decreased. Thus, the addition of a secondary phase to the PVDF matrix can partially transform the α phase into the β phase. [12] It is well known that the PVDF's polar β phase leads to better dielectric properties. [13] This phase is also responsible for the piezoelectric and pyroelectric properties, and it is strongly

dependent on the preparation and the polarization processing. [14-16] FT-IR spectroscopy gives a detailed view of the PVDF/carbon composite foams' exact phase formations, as is shown in Figure S4 (b and d). Both the PVDF/CNTs and the PVDF/GnP composite foams had similar FT-IR spectra. In other words, all of the PVDF/carbon composite foams consisted of both the α-phase and the β-phase. The α-phase was observed at 766, 795, and 975 cm^{-1}. The absorbance bands at 765 cm^{-1} were attributed to the rocking vibration of the CF_2 in the PVDF chain. [15, 17] The absorbance bands at 840, 872, 1,171, and 1,275 cm^{-1} were assigned to the β phase. [18] The in plane bending or scissoring of the CH_2 was observed at 1,402 cm^{-1} while the C–C–C bending appeared at 1,070 cm^{-1}. [10] On the basis of the XRD and FT-IR results, we concluded that the introduction of a second phase had affected the crystalline phase of the PVDF from the α-phase to the β-phase, and that the PVDF/carbon composite foams had consisted of both phases.

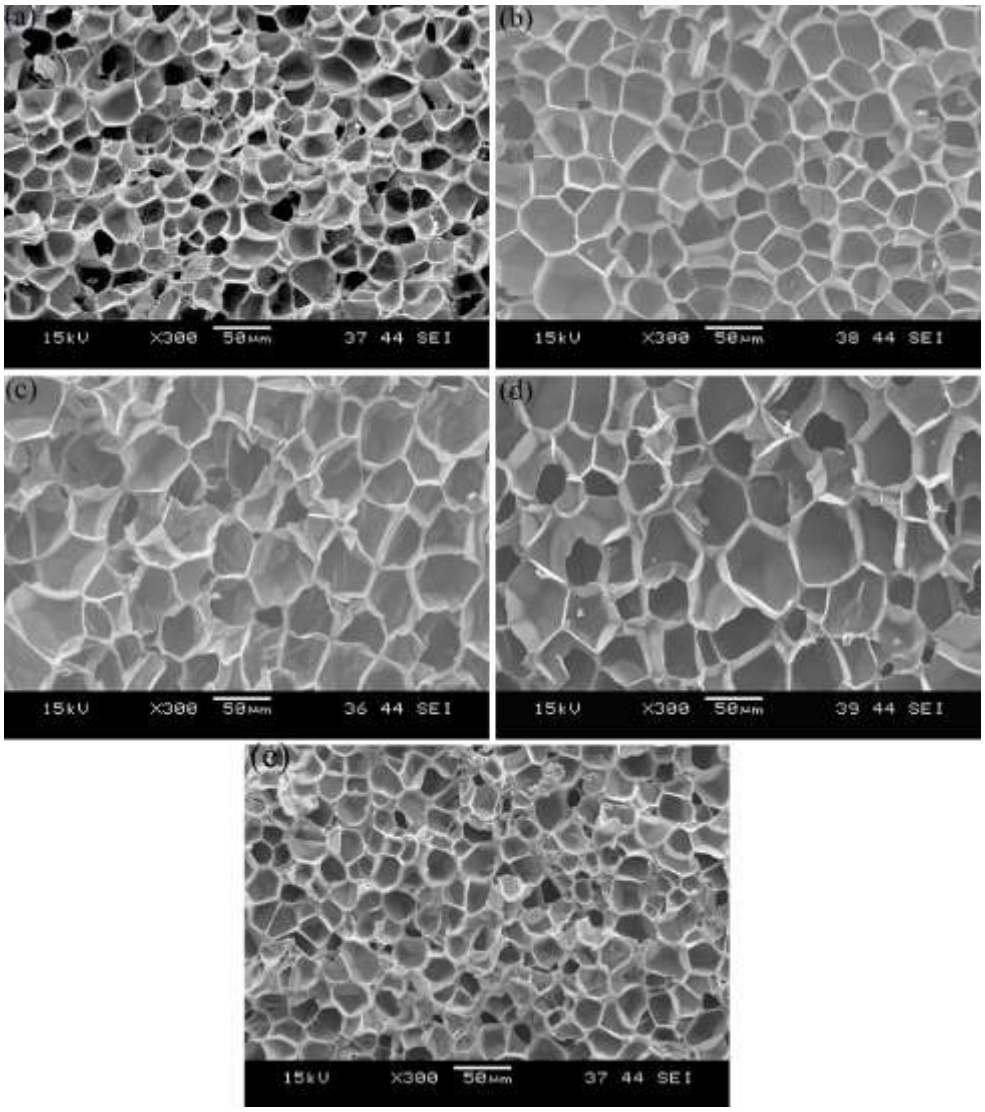

Figure S5. SEM micrographs of various PVDF/CNT composite foams: (a) FN1, (b) FN2, (c) FN3, (d) FN4, and (e) FN5

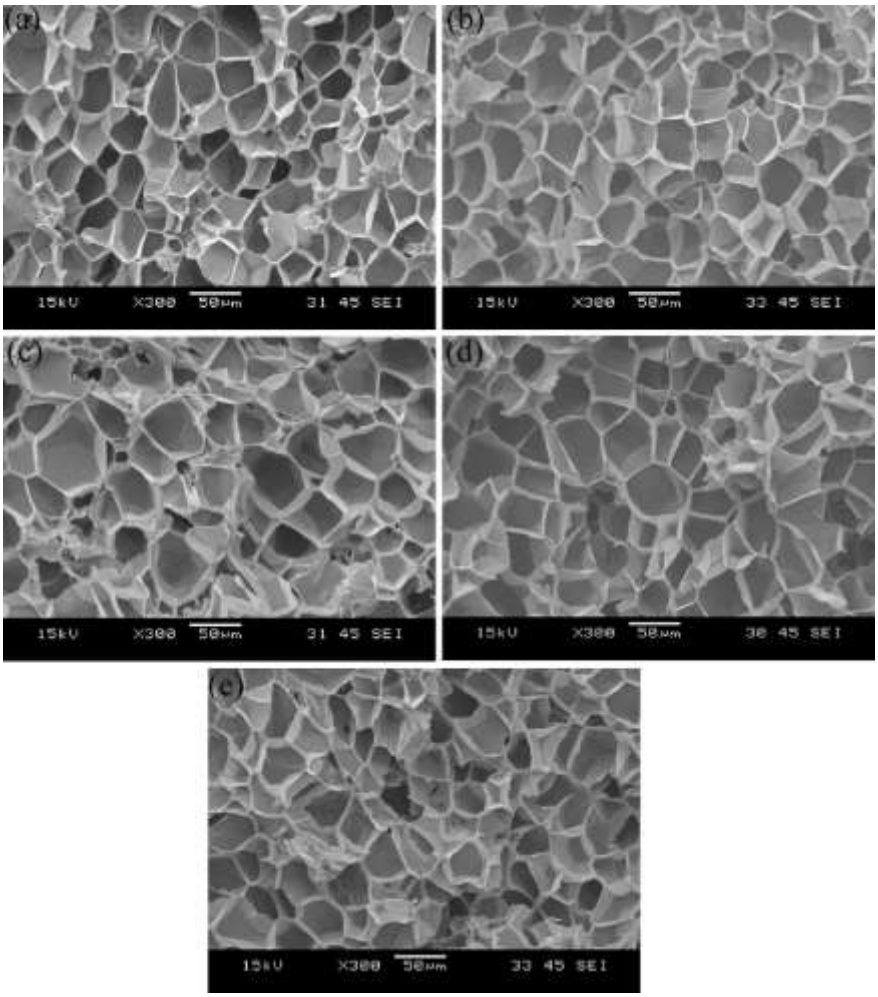

Figure S6**.** SEM micrographs of various PVDF/GnP composite foams: (a) FG1, (b) FG2, (c) FG3, (d) FG4, and (e) FG5.

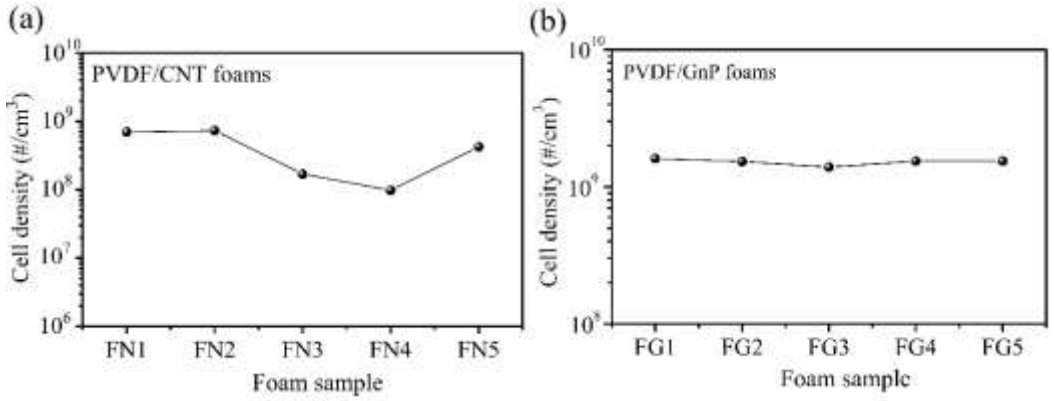

Figure S7 The cell density of (a) PVDF/CNT composite foams and (b) PVDF/GnP composite foams.

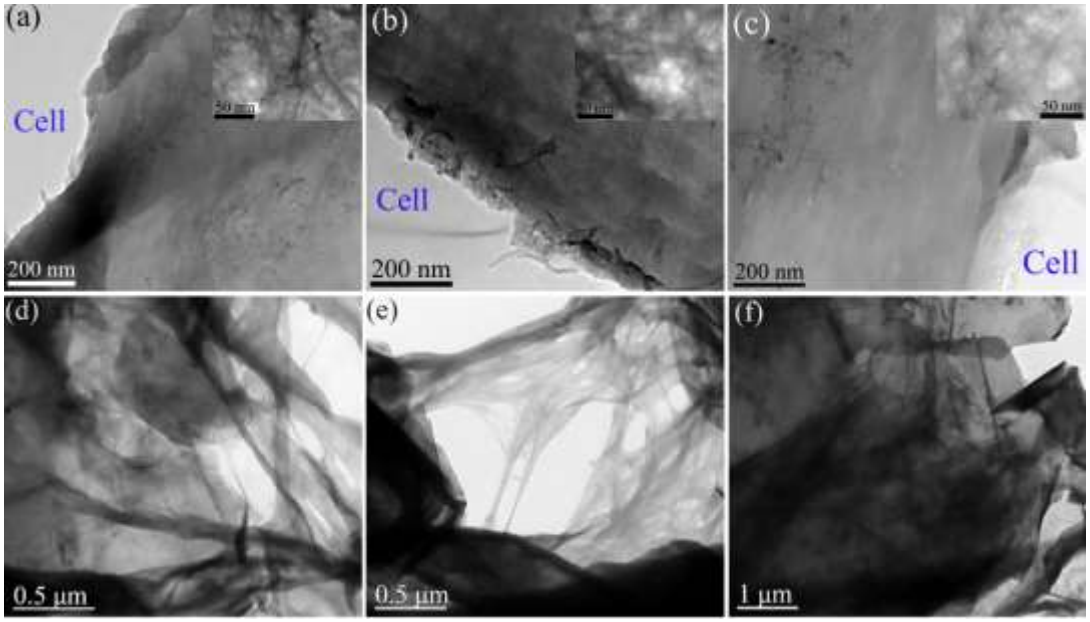

Figure S8 (a-c) TEM images captured on the foam walls of FN1-FN3 samples; (d-f) TEM images obtained on the foam walls of FG1-FG3 samples. The insets in Figure S8 (a-c) are the correponding high magnification TEM images of FN1-FN3 samples.

Reference:

1. B. Zhao, C. Zhao, R. Li, S. M. Hamidinejad and C. B. Park, *ACS Appl. Mater. Interfaces*, 2017, **9**, 20873-20884.
2. B. Zhao and C. B. Park, *J. Mater. Chem. C*, 2017, **5**, 6954-6961.
3. L. Huang, C. Lu, F. Wang and L. Wang, *RSC Adv.*, 2014, **4**, 45220-45229.
4. J. W. S. Lee, R. E. Lee, J. Wang, P. U. Jung and C. B. Park, *Chem. Eng. Sci.*, 2017, **167**, 105-119.
5. X. Xu, C. B. Park, D. Xu and R. Pop-Iliev, *Polym. Eng. Sci.*, 2003, **43**, 1378-1390.
6. A. Ameli, M. Nofar, S. Wang and C. B. Park, *ACS Appl. Mater. Interfaces*, 2014, **6**, 11091-11100.
7. A. Ameli, M. Nofar, C. B. Park, P. Pötschke and G. Rizvi, *Carbon*, 2014, **71**, 206-217.
8. A. Ameli, S. Wang, Y. Kazemi, C. B. Park and P. Pötschke, *Nano Energy*, 2015, **15**, 54-65.
9. M. Hamidinejad, B. Zhao, R. K. M. Chu, N. Moghimian, H. E. Naguib, T. Filleter and C. B. Park, *ACS Appl. Mater. Interfaces*, 2018, **10**, 19987-19998.
10. B. Zhao, C. Zhao, C. Wang and C. B. Park, *J. Mater. Chem. C*, 2018, **6**, 3065-3073.
11. H.-D. Huang, C.-Y. Liu, D. Zhou, X. Jiang, G.-J. Zhong, D.-X. Yan and Z.-M. Li, *J. Mater. Chem. A*, 2015, **3**, 4983-4991.
12. G. Wang, L. Wang, L. H. Mark, V. Shaayegan, G. Wang, H. Li, G. Zhao and C. B. Park, *ACS Appl. Mater. Interfaces*, 2018, **10**, 1195-1203.
13. B. Dai, B. Zhao, X. Xie, T. Su, B. Fan, R. Zhang and R. Yang, *J. Mater. Chem. C*, 2018, **6**, 5690-5697.
14. G. Sun, X. Zhang, M. Cao, B. Wei and C. Hu, *J. Phys. Chem. C*, 2009, **113**, 6948-6954.
15. M.-P. Tran, C. Detrembleur, M. Alexandre, C. Jerome and J.-M. Thomassin, *Polymer*, 2013, **54**, 3261-3270.
16. B. Luo, X. Wang, Y. Wang and L. Li, *J. Mater. Chem. A*, 2014, **2**, 510-519.
17. B. Wen, M. Cao, M. Lu, W. Cao, H. Shi, J. Liu, X. Wang, H. Jin, X. Fang, W. Wang and J. Yuan, *Adv. Mater.*, 2014, **26**, 3484-3489.
18. J. Liang, Y. Wang, Y. Huang, Y. Ma, Z. Liu, J. Cai, C. Zhang, H. Gao and Y. Chen, *Carbon*, 2009, **47**, 922-925.